East European Journal of Physics. **3.** 194-208 (2025)
DOI:10.26565/2312-4334-2025-3-17 ISSN 2312-4334

INFLUENCE OF LORENTZ FORCE AND ARRHENIUS ACTIVATION ENERGY ON RADIATIVE BIO-CONVECTIVE MICROPOLAR NANOFLUID FLOW WITH MELTING HEAT TRANSFER OVER A STRETCHING SURFACE

Syed Fazuruddin[a], Sreenivasulu Arigela[b]*, A. Shobha[c], V. Raja Rajeswari[d], K. Venkatadri[b#]
[a]*Department of School of Technology Mathematics, The Apollo Knowledge City Campus Saketa, Murukambattu, The Apollo University Chittoor, Andhra Pradesh-517127, India*
[b]*Department of Mathematics, School of Liberal Arts and Sciences, Mohan Babu University (Erstwhile Sree Vidyanikethan Engineering College), Sree Sainath Nagar, Tirupati, A.P., 517102, India*
[c]*Department of Applied Mathematics, Sri Padmavathi Mahila Visva Vidyalyam, Tirupati 517502, AP, India*
[d]*Department of Electronics and Communication Engineering, School of Engineering and Technology, Sri Padmavathi Mahila Visva Vidyalayam, Tirupati 517502, A.P., India*
**Corresponding Author E-mail: sreenu1184@gmail.com; [#]E-mail: venkatadri.venki@gmail.com*
Received July 1, 2025; revised August 7, 2025; accepted August 15, 2025

Novelty of this research is to explore an impact of Lorentz force, Arrhenius activation energy, and Conduction of Melting Heat on the micropolar fluid behaviour of steady radiative bio-convective micropolar nanofluid flow towards a stretchable surface. Using the standard similarity method, we have derived the equations of similarity for the relevant quantities of momentum, angular momentum, temperature, and concentration. The MATLAB tool 'bvp4c' is used to determine solutions to the transformed governing equations. Equations of similarity in four dimensions (momentum, angular momentum, temperature, and concentration) are numerically solved. We have examined, microrotation, velocity, concentration, temperature fields behavior for various parameters. Results show that the motile density of microorganisms decreases when the Peclet number and the microorganism concentration differential parameter are increased. Motility density increases as the Peclet number in microbial concentrations rises. Nanofluids are therefore appropriate as heat transfer fluids due to their surface cooling effect. The numerical scheme applied is validated by comparison with the previous numerical values.

Keywords: *Melting Heat Transfer; Micropolar nanofluid; Bioconvection; Radiative heat flux; Activation energy*
PACS: 44.05.+e, 47.11.-j, 41.20.-q, 47.15.Rq, 47.65.-d, 47.55.pb, 44.30.+v

Nomenclature

K	*Material parameter*	***C***	*concentration*
Rd	*Thermal radiation parameter*	***Cw***	*Concentration at the surface*
Pr	*Prandtal number*	***C∞***	*Ambient fluid concentration*
Nb	*Brownian Motion parameter*	***Cp***	*Specific heat*
Nt	*Thermo Phoresis parameter*	***Ds***	*Microorganism diffusion coefficient*
Ec	*Eckert Number*	***f***	*Dimension less stream function*
Le	*Lewis number*	***f '***	*Dimension less velocity*
Da	*Darcy number*	***k****	*Mean absorption coefficient*
M	*Magnetic parameter*	***Nu***	*Local Nusselt number*
λ	*Mixed convection parameter*	***Q_0***	*Heat generation/Absorption parameter*
θw	*Temperature Ratio parameter*	***s***	*Microorganism field*
E	*Activation Energy parameter*	***s_w***	*Microorganism at the surface*
Lb	*The Bioconvection Lewis number*	***s_∞***	*Ambient fluid Microorganism*
Pe	*Peclet number*	***Sh***	*Local Sherwood number*
Ω	*The constant difference constant of microorganism*	***T***	*Fluid temperature*
S	*Suction parameter*	***Tw***	*Temperature at the surface*
Ma	*Melting parameter*	***T∞***	*Ambient fluid temperature*
L	*Momentum slip parameter*	***Uw***	*Stretching velocity*
m	*Micro rotation parameter*	***(u, v)***	*Velocity components along x-axis and y-axis respectively*
γ_1	*Thermal Biot number*	***(x, y)***	*Space coordinates*
γ_2	*Mass Biot number*	***Wc***	*Cell moving speed*
Nr	*Buoyancy Ratio parameter*	***η***	*Dimension less variable*
Nc	*Bioconvection Rayley number*	***μ***	*Dynamic viscosity*
ε	*Variable thermal conductivity parameter*	***σ****	*Stefan-Boltzmann constant*
Re	*Reynolds number*	***ϕ***	*Volumetric concentration*
σ	*Reaction rate parameter*	***χ***	*Microorganism concentration*
a	*Stretching rate*	***ψ***	*Stream function*
Bh	*Local microorganism density number*		

Cite as: S. Fazuruddin, S. Arigela, A. Shobha, V.R. Rajeswari, K. Venkatadri, East Eur. J. Phys. 3, 194 (2025), https://doi.org/10.26565/2312-4334-2025-3-17

As micro-organisms move upward on average, the phenomenon of bioconvection occurs In general, microorganisms have a higher density than water. It is the microorganisms' own self-propelled movement across the upper fluid zone that causes the surface there to thicken to an unstable degree. Exciting circumstances lead to a complex network of currents. Bioconvection is used in a wide variety of fields, but the ones that stand out the most include bio microsystems, biotechnology, environmental systems, biofuels, and petroleum engineering. Using nanoparticles in a bioconvection process calls for the combined properties of buoyant forces and microorganisms. Suspensions containing nanoparticles and gyrotactic microorganisms may grow in a way that is both pleasant and effective in terms of their stability. Microorganisms are often sorted into the chemotactic or oxytactic kind, the gyrotactic, microorganisms, and the geotactic, microorganisms, based on the directions in which they travel. Another key factor in the enhanced stability of nanoparticles is the bioconvection phenomenon. Prokaryotic bacteria move in a variety of ways, including swimming, crawling, gliding, and skimming across solid surfaces and fluid media. Without flagella, rod-shaped bacteria have adapted gliding as a mode of locomotion. Relevant instances include the BH3 stain from Flexibacter, as well as cytophaga, oscillatoria, and vitreoscilla. Bioconvection, or the diffusion of lower denseness microorganisms near surface liquid, results in the emergence of stable, chaotic patterns. Algae and other freely moving microorganisms have a tendency to cluster together in the fluid's top layer, where they might contribute to the stratification density and harden the surface. When compared to microbes, nanomaterials move in a way that is distinct. It is essential for microfluidics that bioconvection and water nanofluids interact. There is a significant challenge in developing microfluidic devices due to the mobility of microbes. Maintaining the bacterium's shape, molecular sieving, and enhancing the bacteria's ability to associate with macrophages [1]. Bacterial motility is greatly aided by the S-layer. An important part of a cell's ability to propel itself forward is its form and the stiffness of its wall and surface layers, both of which are maintained in part by the S-layer. The cell is shielded by the S-layer from harmful ions, acids, osmotic stress, enzymes, viruses, and other bacteria. Their cells may adhere to those of other types or to surfaces. Protection from phagocytosis is something they can provide harmful bacteria. Soil, silt, and rotting wood are just a few examples of watery environments that bacteria may adapt to grow in through tiny channels that allow them to glide [2]. Gliding motility, namely its mechanism, is still a matter of some controversy. Circulating discs on the surface of the cells, electro-kinesis, the release of slime, the application of osmotic pressures, the generation of peristaltic waves on the surface, and contractile components are all mentioned in the literature as contributing to bacterial motility [3, 4]. To explain the vitreoscilla's glide-like movement, Costerton et al. [5] proposed this theory. In their paper, Halfen and Castenholz [6] hypothesised that the wavy regime, that is virtually in touch with solid barrier and allows green-blue algae’s to glide with such ease. That flexibacter may move by sending off waves from its own surface was substantiated by research published by Humphrey et al. [7]. As one of two mechanisms used by cyanobacteria for locomotion, Hoiczyk [8] described the formation of tiny surface waves that flow along the surface of the filament. Because of these observations, Venkatadri et al. [9] presents a novel investigation of thermomagnetic bioconvection flow involving oxytactic microorganisms within a semi-trapezoidal porous enclosure, particularly targeting magnetic biofuel cell applications. The coupling of magnetic fields, bioconvection, porous media effects, and nanofluid transport offers a strong precedent for studies focusing on multiphysics transport phenomena in non-standard enclosures, especially in contexts involving thermal energy harvesting or biological systems. O'Brien [10] decided to create a mathematical model to investigate bacterial glide behaviour. Using lubrication theory, he determined the flexibacter's maximum speed and the rate at which power was dissipated. They used those findings to suggest a model for Flavobacterium gliding, and the math behind it seems sound. Islam and Mignot [11] analyse in depth the role of focal adhesions in the pathogenesis of Myxococcus xanthus. An outstanding review study on the gliding processes described in flavobacteria, myxobacteria, mycoplasmas literature was published by Nan and Zusman [12]. An effects of heat and mass transmission, as well as the mobility of microorganisms, on the motion of a nanofluid were examined by Shafiq et al.[13]. When it comes to the boundary layer flow containing gyrotactic nano liquid microorganisms, Elbashbeshy et al.[14] used computational methods to examine the impact of heat production across an incline stretched cylinder. Using computational methods, we examine the bioconvection of a nanofluid via a stretched surface in a porous media containing gyrotactic microorganisms subject to Newtonian heating reported by Pourrajab and Noghrehabadi [15]. In this paper, we investigate the effect of thermosolutal Marangoni on bioconvection in a solution of gyrotactic microorganisms over an inclined stretched sheet explored by Kairi et al. [16]. Compliant thermoelectric coils for use in flexible and biointegrated devices are analysed for thermal and mechanical properties explored by Chen et al. [17]. Over a vertical cone, a numerical solution is found for bioconvection in convectional nanofluid flow including gyrotactic microorganisms explored by Rao et al. [18].

Some fluids, due to the micromotions of their constituent parts, display microscopic phenomena that are the focus of the idea of micropolar fluid. A diluted suspension of stiff macromolecules, each with its own movements supporting stress and body moments and governed by spin inertia, may be found in these fluids. Some fluids, known as micropolar fluids, have notably non-Newtonian hydrodynamics due to the existence of micro-constituents that are capable of rotation. Micropolar fluid, one of numerous types of non-Newtonian fluids, is best suited to characterising both the microstructure-determined local characteristics and the intrinsic particles liquid movement. As a result of these features, micropolar fluid modeling problems widely utilised to mimic complicated processes in a wide variety of liquids, such as polymer, plastic planes, ferrofluid, crystals, biology, etc. Thermo-micropolar fluids theory was developed by Eringen [19], who also created the theory of micropolar fluids and obtained its constitutive equations. In essence, Eringen is responsible for developing the idea of micropolar fluids. Many different kinds of fluids, from suspension solutions to blood rheology and

colloidal fluids, may be studied mathematically with the help of this model. Polymer fluids, liquid suspension, blood, crystals, dusty cloud, etc. includes micropolar liquids (Ahmadi [20]; Hayat et al. [21]). Researchers' curiosity with it has been piqued by the wide variety of industrial processes in which it is used, including polymer extrusion, lubricants, water baths are used to cool metallic plates (Rahman [22]). Lukaszewicz [23] explained a comprehensive theory, micropolar liquids applications.

Phenomenon of melting heat transfer is fundamentally important in many technological and industrial endeavors, such as understanding permafrost melting, magma-solidifications, metal-purifications, etc. Epstein and choi et al. [24] found that melting affects heat transmission process. In a micropolar fluid, Yacob et al. [25] studied heat melting transfer at the stagnation point of the boundary layer as it moved towards a stretching/shrinking sheet. Powell-Eyring flow with linear surface and heat melting transfer was investigated by Hayat et al. [26]. Khan et al. [27] studied an impact of non-Newtonian flow over a stretched surface on melting heat and mass transfer with non-linear radiation and a magnetic regime. Gireesha et al. [28] proposed MHD flow Casson liquid across a stretched plane at melting heat transfer.

Based on the research that has been done so far, melting stretching sheets have a small number of investigations of MHD Micro-Polar fluid. Revisions to micropolar fluids with gyrotactic microorganisms have received very little attention, as shown by the literature review and by the necessary engineering and industrial applications. An objective of this manuscript is to explore an impact of Lorentz force, Arrhenius activation energy, and Conduction of Melting Heat on the micropolar fluid behavior of steady radiative bio-convective micropolar nanofluid flow towards a stretchable surface. The results of changing any of the controlling variables may be seen in graphical form. Further research in the fields of fuel production, crushed water flow issues, and polymer sheet extrusion may all benefit from the analyses provided in the cited study. Engineering designs, metallurgy industries, and the effectiveness of systems for the flow of thermos fluids all benefit from the findings of this research. Biomedical, industrial, pharmaceutical, and thermal/thermal processes may all benefit greatly from this design.

2. MATHEMATICAL CONCEPTUALIZATION

This integrated study constitutes self-motivated bio-convective microorganisms, numerous slips, non-linear radiative micropolar nano fluids. Flow of a fluid, often considered to be laminar, two-dimensional, and incompressible. Figure 1. depicts flow model of the problem. In order to properly evaluate an induced magnetic influence, a high magnetic Reynolds number is required.

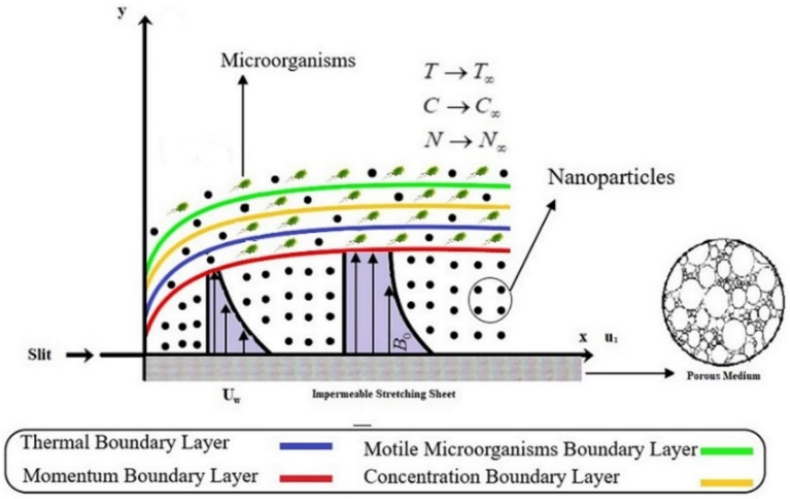

Figure 1. Flow Model

Additionally, the flow is assumed to be a steady-state flow during the development of the model. Velocity of surface material is $U_w = ax$, a is positive. All these factors taken into account, the governed boundary equations are as follows:

$$\frac{\partial u}{\partial x}+\frac{\partial v}{\partial y}=0 \tag{1}$$

$$u\frac{\partial u}{\partial x}+v\frac{\partial u}{\partial y}=\left(\frac{\mu+k}{\rho}\right)\frac{\partial^2 u}{\partial y^2}+\frac{k}{\rho}\frac{\partial N}{\partial y}-\frac{\sigma B_0^2}{\rho}u-\frac{\upsilon}{\kappa}u + g\beta_T\left[T-T_\infty\right]+g\beta_C\left[C-C_\infty\right]+g\beta_s\left[s-s_\infty\right] \tag{2}$$

$$u\frac{\partial N}{\partial x}+v\frac{\partial N}{\partial y}=\frac{\gamma}{\rho j}\frac{\partial^2 N}{\partial y^2}-\frac{\kappa}{\rho j}\left[2N+\frac{\partial u}{\partial y}\right] \tag{3}$$

$$u\frac{\partial T}{\partial x}+v\frac{\partial T}{\partial y}=\alpha\left(\frac{\partial^2 T}{\partial y^2}\right)-\frac{1}{\rho C_p}\frac{\partial q_r}{\partial y}+\tau\left(D_B\frac{\partial C}{\partial y}\frac{\partial T}{\partial y}+\frac{D_T}{T_\infty}\left(\frac{\partial T}{\partial y}\right)^2\right)+\left(\frac{\mu+k}{\rho C_p}\right)\left(\frac{\partial u}{\partial y}\right)^2+\frac{Q_0}{\rho C_p}[T-T_\infty] \tag{4}$$

$$u\frac{\partial C}{\partial x}+v\frac{\partial C}{\partial y}=D_m\left(\frac{\partial^2 C}{\partial y^2}\right)+\frac{D_T}{T_\infty}\frac{\partial^2 T}{\partial y^2}-k_c\left(C-C_\infty\right)\left(\frac{T}{T_\infty}\right)^n\exp\left(\frac{-E_a}{k_a T}\right) \tag{5}$$

$$u\frac{\partial s}{\partial x}+v\frac{\partial s}{\partial y}+\frac{bW_c}{\left(C_w-C_\infty\right)}\left[\frac{\partial}{\partial y}\left(s\frac{\partial C}{\partial y}\right)\right]=D_s\left(\frac{\partial^2 s}{\partial y^2}\right) \tag{6}$$

Convective boundary conditions

$$\begin{aligned}&u=U_w+L_1\frac{\partial u}{\partial y},\\&v=k\frac{1}{\rho\left[\beta_m+c_s\left(T_m-T_0\right)\right]}\frac{\partial T}{\partial y}-v_w\\&N=-m\frac{\partial u}{\partial y},-k\frac{\partial T}{\partial y}=h_f\left(T-T_w\right),-k\frac{\partial C}{\partial y}=h_m\left(C-C_w\right),s=s_w\end{aligned} \tag{7}$$

$$u\to 0,N\to 0,T\to T_\infty,C\to C_\infty,s\to s_\infty \tag{8}$$

$$\gamma=\left(\mu+k/2\right)j=\mu\left(1+K/2\right),\qquad K\ \textit{denotes the material parameter}$$

Thermal conductivity as a function of temperature is defined as

$$k=k_\infty\left(1+\varepsilon\frac{T-T_\infty}{T_w-T_\infty}\right)$$

A usual stream functions

$$u=\frac{\partial\psi}{\partial y}\ \text{and}\ v=-\frac{\partial\psi}{\partial x} \tag{9}$$

Considering similarity transformations are

$$\begin{aligned}&u=axf',v=-\sqrt{av}f(\eta),\eta=y\sqrt{\frac{a}{\upsilon}},\psi=x\sqrt{av}f(\eta),\theta(\eta)=\frac{T-T_\infty}{T_w-T_\infty},\\&\phi(\eta)=\frac{C-C_\infty}{C_w-C_\infty},T=T_\infty\left[1+\left(\theta_w-1\right)\theta\right],\ \chi(\eta)=\frac{s-s_\infty}{s_w-s_\infty},\theta_w=\frac{T_w}{T_\infty},\end{aligned} \tag{10}$$

Non-linear Radiative heat flux

$$q_r=-\frac{4\sigma^*}{3k^*}\frac{\partial T^4}{\partial y} \tag{11}$$

$$\frac{\partial q_r}{\partial y}=-\frac{16\sigma^*}{3k^*}\left[3T^2\left(\frac{\partial T}{\partial y}\right)^2+T^3\frac{\partial^2 T}{\partial y^2}\right] \tag{12}$$

Converted ODEs are

$$\left[1+K\right]f'''-f'^2+ff''+Kg-Daf'-Mf'+\lambda\left(\theta-Nr\phi-Nc\chi\right)=0 \tag{13}$$

$$\left[1+\frac{K}{2}\right]g''+fg'-f'g-K\left[2g+f''\right]=0 \tag{14}$$

$$\begin{aligned}&\left[\left(1+\varepsilon\theta\right)+\frac{4}{3}Rd\left(1+\left(\theta_w-1\right)\theta\right)^3\right]\theta''+\left[\varepsilon+4Rd\left(\theta_w-1\right)\left(1+\left(\theta_w-1\right)\theta\right)^2\theta'^2\right]\\&+\Pr f\theta'+\Pr\left(Nb\theta'\phi'+Nt\theta'^2\right)+Ec\Pr\left(f''\right)^2+\Pr Q_0\theta=0\end{aligned} \tag{15}$$

$$\phi''+\Pr Lef\phi'+\left(\frac{Nt}{Nb}\right)\theta''-\Pr Le\sigma(1+\delta\theta)^{n}\exp\left(\frac{-E}{1+\delta\theta}\right)\phi=0 \tag{16}$$

$$\chi''+Lbf\chi'-Pe\left[\phi''(\chi+\Omega)+\phi'\chi'\right]=0 \tag{17}$$

The relative boundary conditions are

$$\begin{aligned} &f(0)=S-\frac{Ma}{\Pr}\theta'(0),f'(0)=1+Lf''(0),\ g(0)=-mf''(0),\\ &\theta'(0)=-\gamma_1(1-\theta(0)),\phi'(0)=-\gamma_2(1-\phi(0)),\ \chi(0)=1 \end{aligned} \tag{18}$$

$$f'(\infty)=0,g'(\infty)=1,h\to 0,\theta(\infty)=0,\phi(\infty)=0,\chi(\infty)=0 \tag{19}$$

The relation of flow transformations:

$$\begin{aligned} &\lambda=\frac{Gr_T}{\mathrm{Re}_x^2},\delta=\frac{Gr_C}{\mathrm{Re}_x^2},\gamma=\frac{Gr_s}{\mathrm{Re}_x^2},Gr_T=\frac{g\beta_T(T_w-T_\infty)x^3}{\upsilon^2},Gr_C=\frac{g\beta_C(C_w-C_\infty)x^3}{\upsilon^2},\\ &Gr_s=\frac{g\beta_s(s_w-s_\infty)x^3}{\upsilon^2},Rd=\frac{16\sigma^*T_\infty^3}{3kk^*},Sc=\frac{\upsilon}{D_B},Lb=\frac{\upsilon}{D_s},Pe=\frac{bW_c}{D_s},\\ &\varepsilon=\frac{\upsilon}{\alpha_e},\ \Omega=\frac{s_w}{s_w-s_\infty},Q=\frac{Q_0}{a\rho C_p} \end{aligned}$$

Where $\lambda_1=L_1\sqrt{\frac{a}{\upsilon}}$, $\lambda_2=L_2\sqrt{\frac{a}{\upsilon}}$, $\lambda_3=L_3\sqrt{\frac{a}{\upsilon}}$, $\lambda_4=L_4\sqrt{\frac{a}{\upsilon}}$

The physical quantities of Cfx, Csx, Nux, Shx are assumed as:

$$Cf=\frac{(\tau_w)_{y=0}}{\rho U_w^2},Cs=\frac{xM_w}{\mu ja},Nu=\frac{x(q_w)_{y=0}}{k[T_w-T_\infty]},Sh=\frac{x(j_w)_{y=0}}{D_M[C_w-C_\infty]},Bh=\frac{x(p_w)_{y=0}}{D_s[s_w-s_\infty]} \tag{20}$$

Where

$$\begin{aligned} &(\tau_w)_{y=0}=\mu\left[\frac{\partial u}{\partial y}\right]_{y=0}+K\left(\frac{\partial u}{\partial y}+N\right)_{y=0},(q_w)_{y=0}=-k\left[\frac{\partial T}{\partial y}\right]_{y=0}+(q_r)_{y=0},\\ &(j_w)_{y=0}=-D_B\left[\frac{\partial C}{\partial y}\right]_{y=0},(p_w)_{y=0}=-D_s\left[\frac{\partial s}{\partial y}\right]_{y=0} \end{aligned} \tag{21}$$

The non-dimensional quantities are

$$\begin{aligned} &\mathrm{Re}_x^{-\frac{1}{2}}Cf=f''(0)(1+M_\lambda)\left(1+\frac{1}{C_\beta}\right),\mathrm{Re}_x^{-\frac{1}{2}}Cs=\left[1+\frac{K}{2}\right]h'(0),\\ &\mathrm{Re}_x^{-\frac{1}{2}}Nu=-\left[1+Nr\theta_w^{*3}\right]\theta'(0),\mathrm{Re}_x^{-\frac{1}{2}}Sh=-\phi'(0),\\ &\mathrm{Re}_x^{-\frac{1}{2}}Bh=-\chi'(0) \end{aligned} \tag{22}$$

Where $\mathrm{Re}_x=\frac{xU_w}{\upsilon}$.

3. NUMERICAL METHOD

Analytical solutions to the modeled equations for a two-point boundary-value problem is impossible because of their extremely nonlinear nature. Computational software MATLAB was used to obtain a numerical solution to this boundary

value problem. In MATLAB, the well-known bvp4c is used to regulate the flow with non-standard parameters. With the help of the MATLAB bvp4c method, numerical results for the dimensionless nonlinearly correlated ODEs, Eqs. (13)-(17) with boundary constraints (18) and (19) are obtained. To solve first-order ODEs, the bvp4c method is used. In this method, the modeled PDEs are transformed into first-order ODEs by taking into account what is appropriate along with boundary conditions, and are then numerically solved using the bvp4c package in MATLAB. The largest allowable residual error and step size are 10^{-6} & $\eta_{\max} = 18$. The approach of the current numerical technique is broken down into its individual components and illustrated in chart form. The flow chart is depicted in Figure 2.

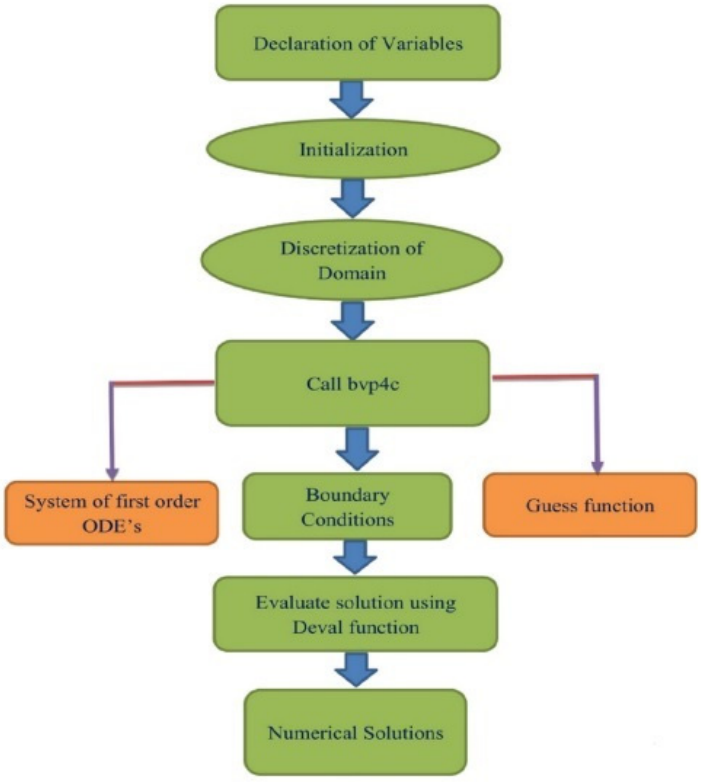

Figure 2. Flow chart of the method of the problem

4. RESULTS AND DISCUSSION:

We have addressed the flow of a viscous, incompressible, micropolar fluid in two-dimensional mixed convective boundary layer through a permeable stretching sheet that is contained in bio-convection, activation energy and melting heat transfer. Assigning numerical values to distinct parameters obtained in the mathematical formulation and displaying the numerical results graphically allows, to gain a physical understanding of the problem by discussing the distributions of velocity $f'(\eta)$, angular velocity $g(\eta)$ (microrotation), temperature $\theta(\eta)$, concentration $\phi(\eta)$ and motile organism $\chi(\eta)$. We have included figures related to local skin friction coefficient τ, couple stress coefficient $h'(0)$, Nusselt number $-\theta'(0)$, Sherwood number $-\phi'(0)$ and micro-organism $-\chi'(0)$.

Figures 3 and 12 shows material parameter K influence in the profiles of f ' (η) and g (η). The microrotation profile exhibits the opposite behaviour, whereas the velocity profile improves as a function of the material parameter. Physically speaking, As the value of the material parameter is raised, the fluid's micro concentration rises, causing a change in the flow, and therefore, the boundary layer thickens. Figures 4 and 13 show how the porosity parameter K affects both the velocity and the angular velocity. Saturated porous medium is the primary focus of this investigation. It is common practice to employ porous medium as insulation for a hot object. Figure 4 shows that when the porosity parameter increases, the velocity decreases. The angular velocity, on the other hand, improves when the porosity parameter rises. This slowing down is explained by the concept of mass conservation and is seen wherever there is an increase in porosity. Figures 5 and 14 show how the velocity and angular velocity change as mixed convection parameter, respectively. Raising mixed convection parameter's value slows air flow. When buoyancy influence on free convection became noticeable, a transition to mixed convection occurs. The buoyancy improves with a raise on mixed convection value. However, when the mixed convection parameter raises, the angular velocity rises along with it. Figures 6 and 15 show the impact of the magnetic field parameter on f ' (η) and g (η). Figure 6 shows that the existence of a magnetic field results in a force called Lorentz, which acts against the flow of the fluid. Figure 15 shows that when the magnetic field strength rises, so does the angular velocity. The Lorentz force, created by the presence of a magnetic field, acts counter to the momentum field in most cases. Increasing the magnetic field has the opposite impact on angular velocity distributions. This is because the

micropolar fluid has elasticity. The results of changing m are shown in Figure 7 for the velocity part. Figure 7 shows that when m rises, both velocity and thickness of the boundary layer reduces. Fig's 8 and 16 depicts Bioconvection Rayleigh number impact on velocity and angular velocity profiles. However, the parameter has inverse behaviours on the microrotation function and the velocity function due to the bioconvection Rayleigh number. The microrotation and fluid flow patterns for different Buoyancy levels are shown in Figures 9 and 17, respectively. It has been shown that increasing the values of buoyancy parameters leads to decreasing the velocity profile and increasing the micro-rotation. The fluid flow and microrotation patterns for distinct values of melting parameter are presented as fig's 10 and 18. When the melting parameter is increased, the fluid flow profile and the microrotation profile are both seen to decrease. Excited by the increased temperature, the fluid's molecules begin to move (as the intermolecular forces that normally keep them together diminish). As the Melting parameter is increased, the micropolar fluid is able to overcome the forces holding its molecules together, allowing it to move faster and decreasing its viscosity gradually as it moves away from the wall. The influence of Prandtl number on the velocity and microrotation fields is seen in Figures 11 and 19. Prandtl number parameter is raised, then fluid's velocity raises and the microrotation profiles near the surface diminish while those distant from the surface improve. Fig. 22 illustrates Prandtl number influence on temperature distribution. Physically, smaller Prandtl number results in a thinner thermal boundary layer and a more uniform temperature distribution. Fig. 20 shows how the temperature ratio parameter affects the temperature distributions seen there. Increasing θw increases both the temperature and related thermal boundary layer thickness. The reason for this is because when w is increased, the fluid temperature becomes much greater than the surrounding ambient temperature. The temperature field for distinct radiation parameter values are shown in Fig. 21. Temperature rises with increasing Rd and the corresponding boundary layer thickness, as seen in the figure. Reason being, a thicker thermal boundary layer and higher temperatures result from an increase in the radiation parameter, which supplies more heat to the fluid. Figure 23 demonstrates that when the Eckert number grows, the sheet temperature rises because of the thermal effect's resistance. Since the Eckert number represents a correlation between kinetic energy and heat enthalpy differences. Therefore, when the Eckert number grows, kinetic energy is converted into internal energy through work against the viscous fluid stresses. Fig. 24 depicts the influence of Brownian motion on temperature distributions. The relationship between temperature and the Brownian parameter is well established. Figure 25 depicts the temperature's response to changing the Thermophoresis parameter. It is clear from these graphs that as Nt grows, so do the temperature profiles. According to the findings, when the Brownian motion parameter is increased, the energy distribution expands, and when the Thermophoresis parameter is increased, the temperature expands. For distinct Thermal Biot number values, the dimensionless temperature profiles are shown in Fig. 26. The fluid temperature rises as the Thermal Biot number (γ_1) increases. Biot number refers ratio of heat conduction resistance within a body to thermal convection resistance on its surface. When a body is heated or cooled over time by a heat flux at the surface, this ratio reveals whether or not the internal temperature fluctuates considerably in space. Concentration fields at various Lewis numbers are seen in Fig. 27. When compared to thermal boundary layer thickness, the concentration boundary layer thins as Le rises. To counteract the lower concentration on boundary layer, a resultant species-induced force diminishes with increasing Le. Figures 28 and 29 show the impact of the controlling factors Nb and Nt on the concentration profile. Brownian motion's effects on the boundary layer concentration of nanoparticles are discussed in Fig. 28. Brownian motion decreases the concentration (variations are minimal for higher values of parameter) and solutal boundary layer thickness, as seen in picture. The concentration of nanoparticles diminishes because an increase in Brownian motion speeds up the random motion that disperses them. Fig. 29 depicts the effects of thermophoresis on the concentration profile. For higher levels of the thermophoresis parameter, this figure shows that the concentration profile declines quickly over the whole flow domain. Given that the random mobility of nanoparticles in liquids is analogous to Brownian motion. As a result of the nanoparticles' erratic motion, the rate at which they collide with molecules in the fluid increases, raising the temperature. Figure 30 demonstrates that the concentration dropped under the effect of the reaction rate parameter. Chemical reactions occur at a rate proportional to the concentration of the reactants, according to the law of mass action. According to this, faster chemical reactions occur when there are higher concentrations of reactants, while slower reactions occur when there are lower concentrations of reactants. Since, parameter δ as it relates to concentration profiles is shown in Figure 31. With an increase in δ, the concentration field weakens. The influence of the activation energy parameter (E) on concentration profile was seen in Fig. 32. The study's authors found that a raise in the 'E' resulted in a corresponding increase on concentration. To initiate a chemical reaction, a quantity of energy called the activation energy presents for chemical system including potentials reactant. In order to determine activation energy, one must first apply Arrhenius equation, that explains a change on rate constants w.r.to temperature. A chemical reaction including a mass transfer phenomenon is used in many fields, including geothermal, chemical, chemistry, emulsions, and deterioration of materials. The connection between chemical processes and the movement of mass is intricate. Both flow fluid and mass transferred studied in relation to one another by manufacturing and digesting species reactant at distinct rates, therefore examining the relationship between the two processes. Concentration profiles are improved by the mass Biot number, as shown in Figure 33. These figures show that when the mass Biot number grows, boundary layer thickness at the solutal concentration also increases. Bioconvection parameter influence is deploy in Figure 34. In order to optimise the bioconvection parameter, the density of gyrotactic, motile microorganisms was decreased. The effect of the Peclet number Pe is seen in Figure 35. The boundary layer thickness of the movable microorganisms has been shown to decrease. The microbes' diffusivity decreases as Pe increases to its maximum value.

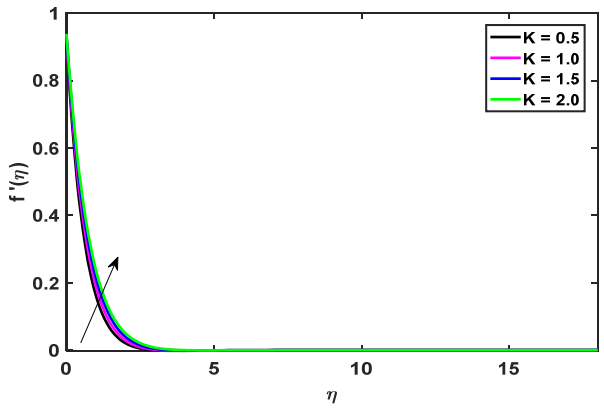

Figure 3. Implementation of K for $f'(\eta)$

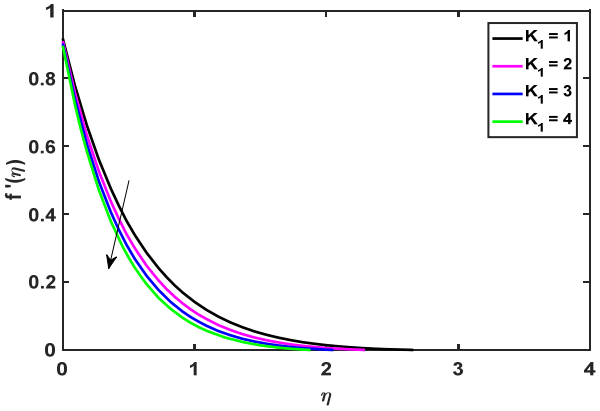

Figure 4. Implementation of K_1 for $f'(\eta)$

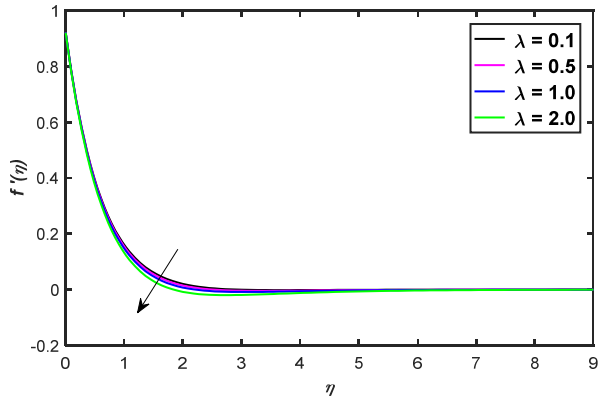

Figure 5. Implementation of λ for $f'(\eta)$

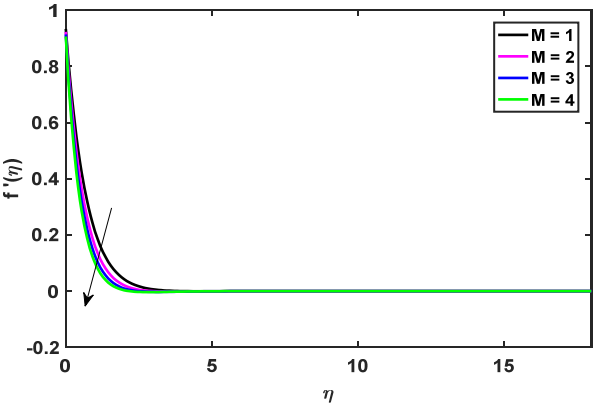

Figure 6. Implementation of M for $f'(\eta)$

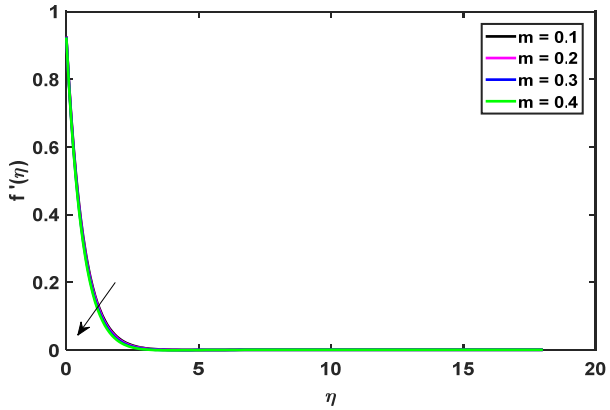

Figure 7. Implementation of m for $f'(\eta)$

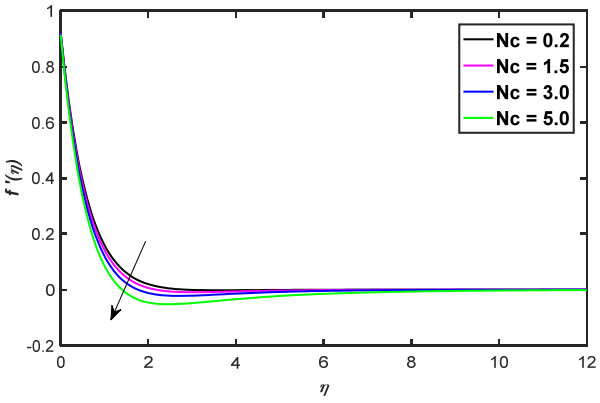

Figure 8. Implementation of Nc for $f'(\eta)$

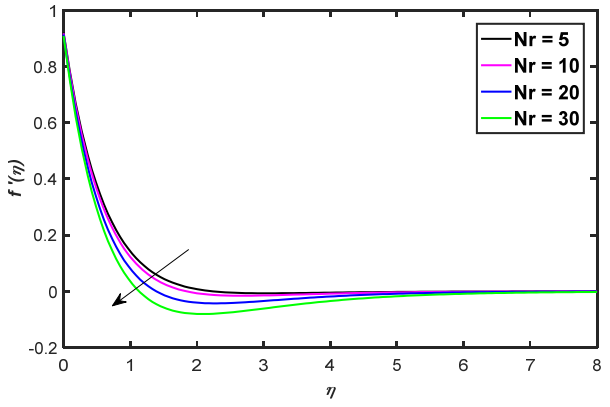

Figure 9. Implementation of Nr for $f'(\eta)$

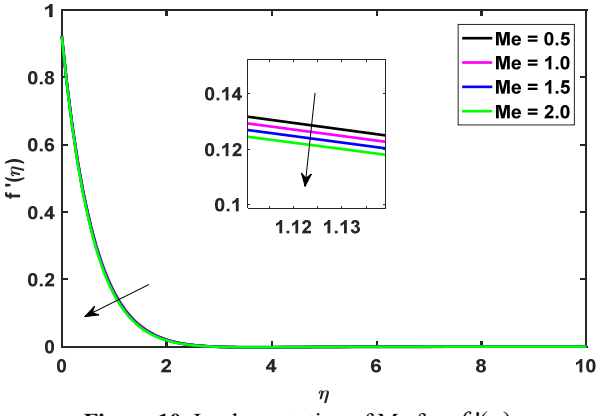

Figure 10. Implementation of Me for $f'(\eta)$

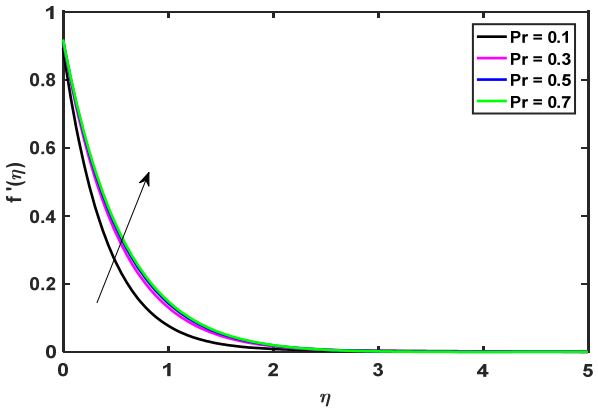

Figure 11. Implementation of Pr for $f'(\eta)$

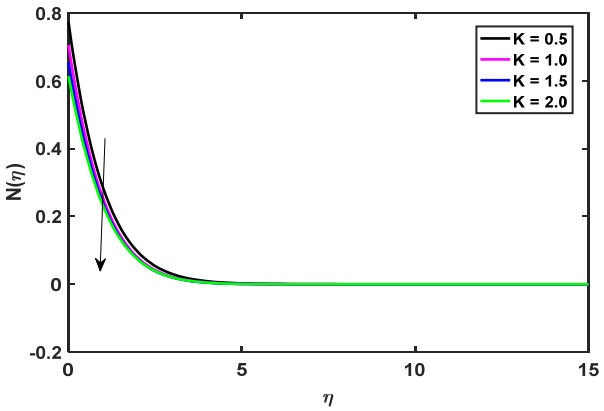

Figure 12. Implementation of K for angular velocity $g(\eta)$

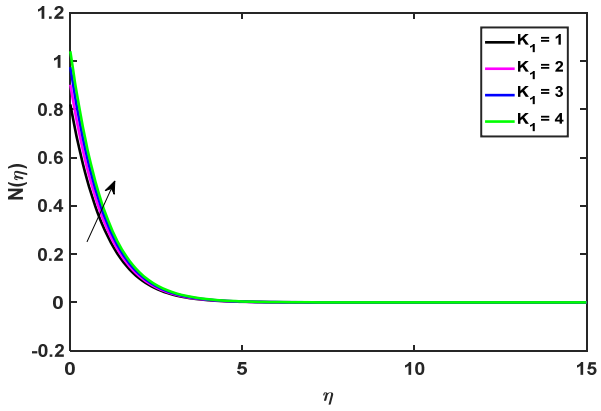

Figure 13. Implementation of K_1 for angular velocity $g(\eta)$

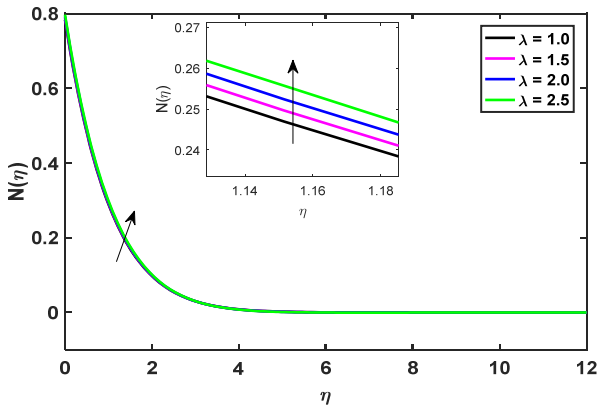

Figure 14. Implementation of λ for angular velocity $g(\eta)$

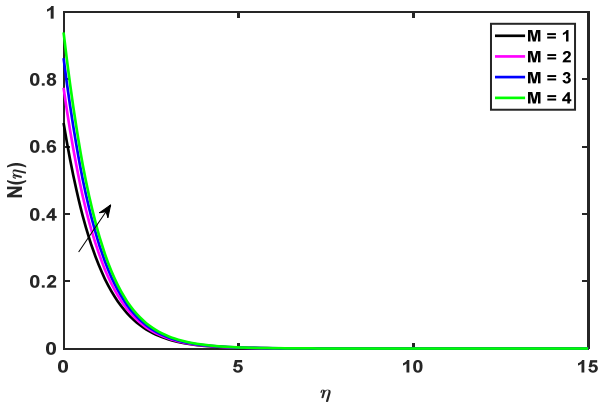

Figure 15. Implementation of M for angular velocity $g(\eta)$

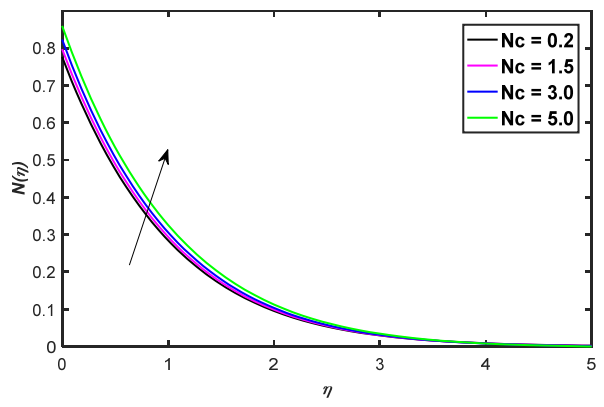

Figure 16. Implementation of Nc for angular velocity $g(\eta)$

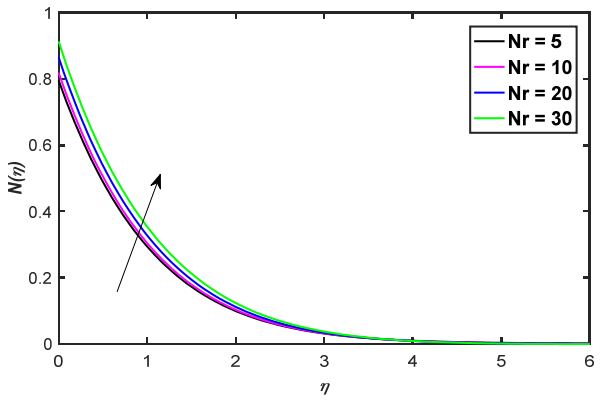

Figure 17. Implementation of Nr for angular velocity $g(\eta)$

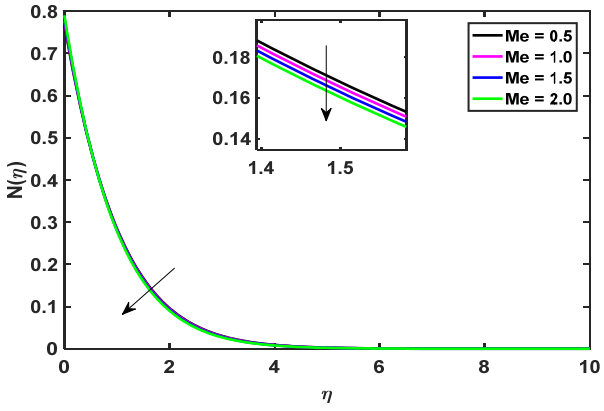

Figure 18. Implementation of Me for angular velocity $g(\eta)$

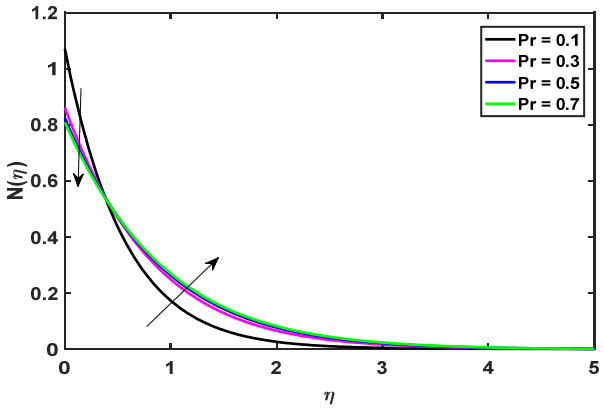

Figure 19. Implementation of Pr for angular velocity $g(\eta)$

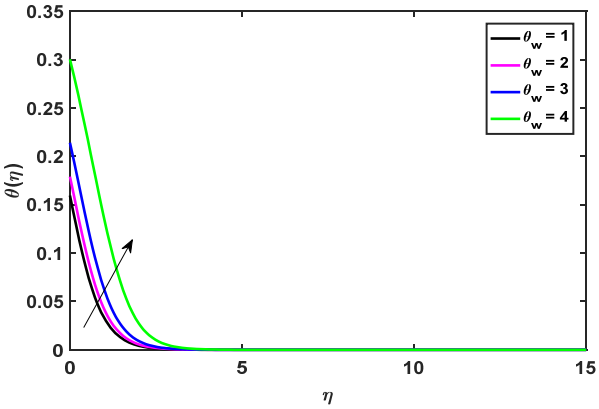

Figure 20. Implementation of θw for $\theta(\eta)$

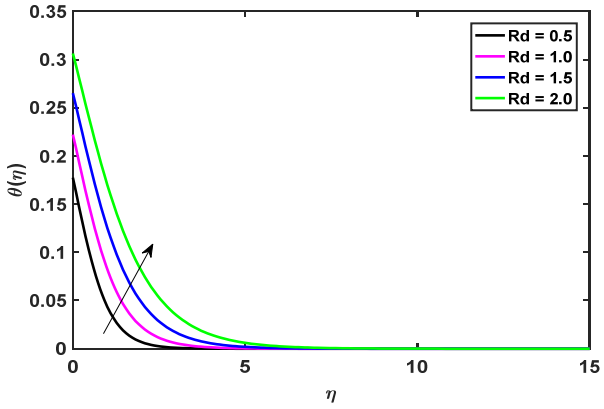

Figure 21. Implementation of Rd for $\theta(\eta)$

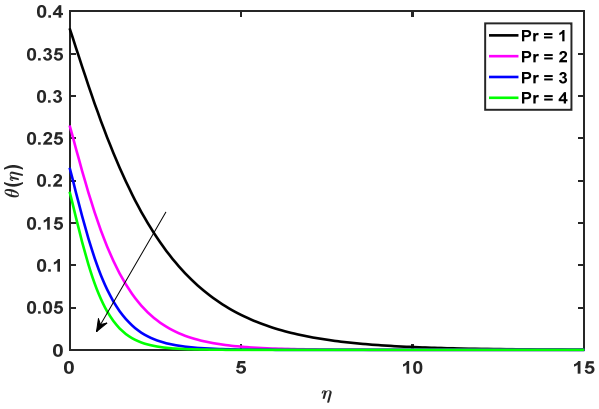

Figure 22. Implementation of Pr for $\theta(\eta)$

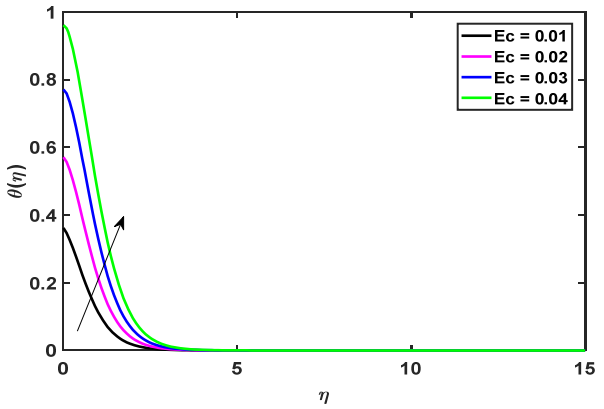

Figure 23. Implementation of Ec for $\theta(\eta)$

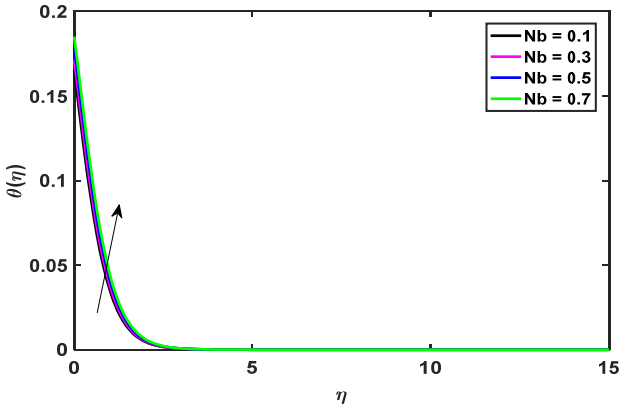

Figure 24. Implementation of Nb for $\theta(\eta)$

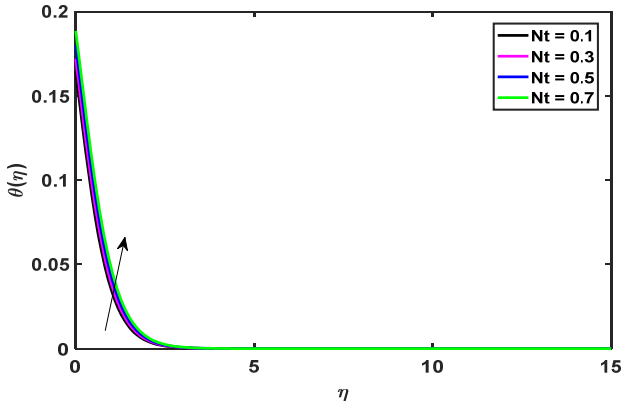

Figure 25. Implementation of Nt for $\theta(\eta)$

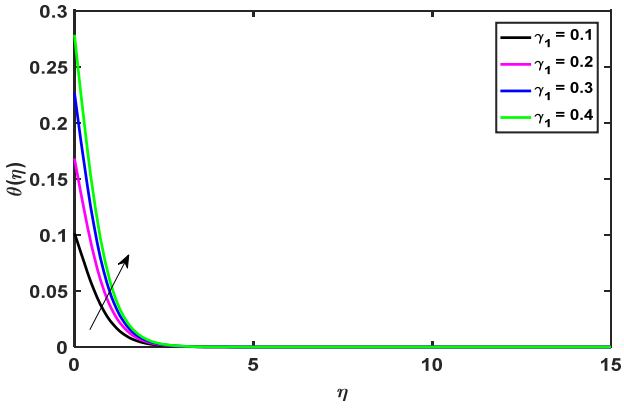

Figure 26. Implementation of λ_1 for $\theta(\eta)$

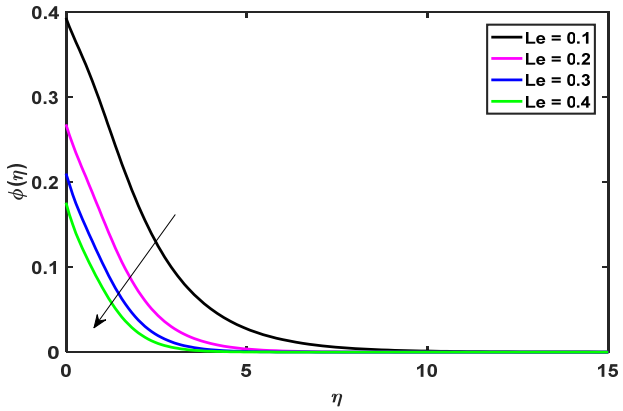

Figure 27. Implementation of Le for $\phi(\eta)$

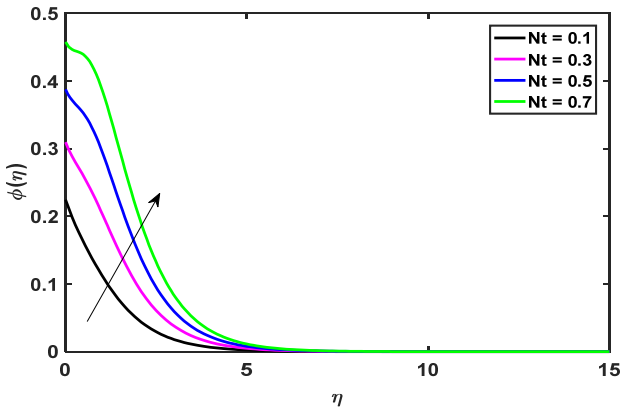

Figure 28. Implementation of Nt for $\phi(\eta)$

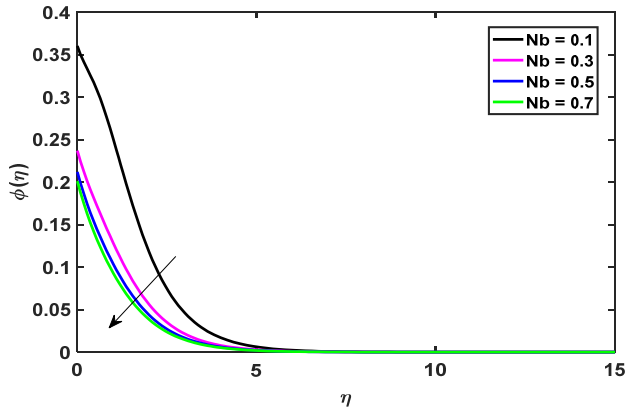

Figure 29. Implementation of Nb for $\phi(\eta)$

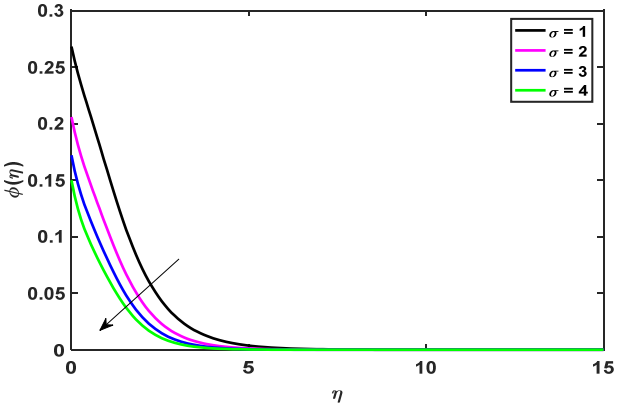

Figure 30. Implementation of σ for $\phi(\eta)$

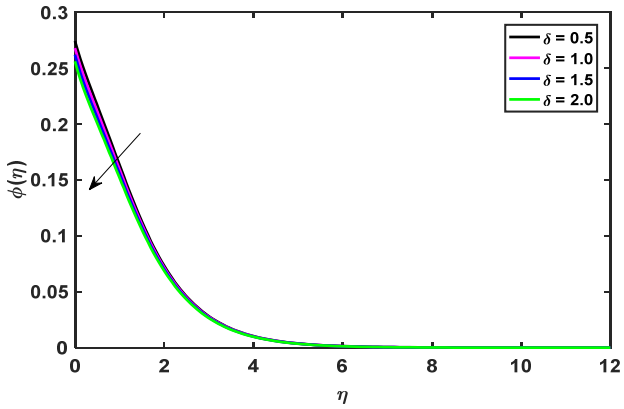

Figure 31. Implementation of δ for $\phi(\eta)$

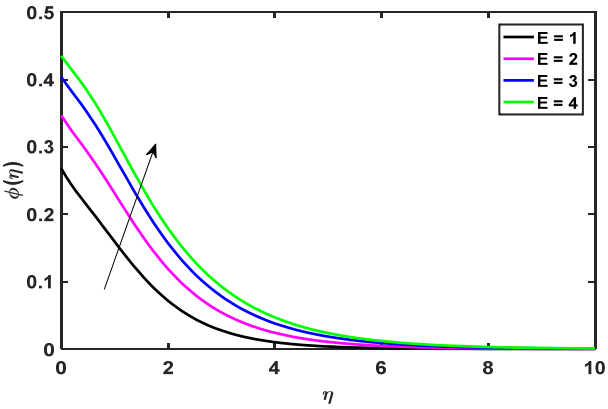

Figure 32. Implementation of E for $\phi(\eta)$

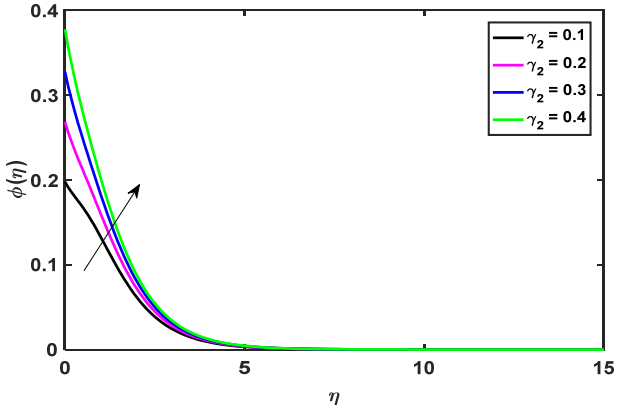

Figure 33. Implementation of λ_2 for $\phi(\eta)$

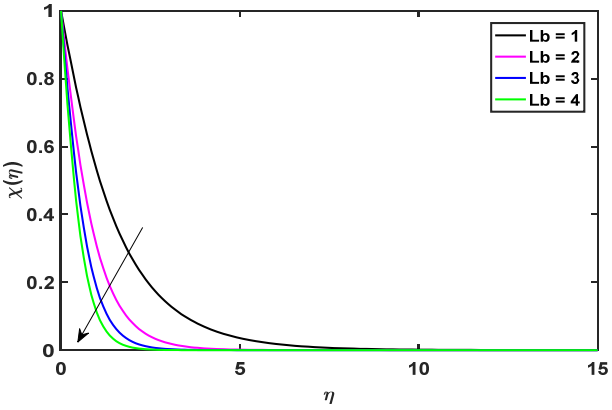

Figure 34. Implementation of Lb for $\chi(\eta)$

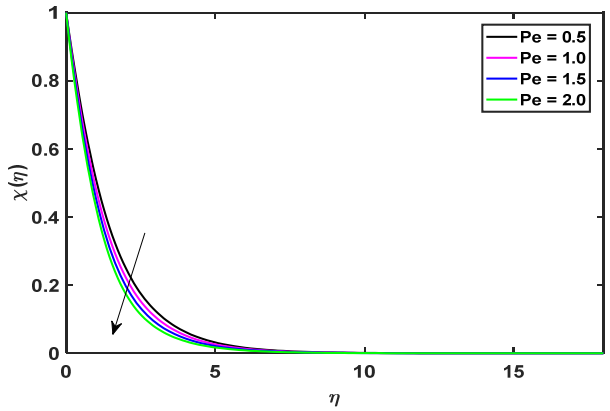

Figure 35. Implementation of Pe for $\chi(\eta)$

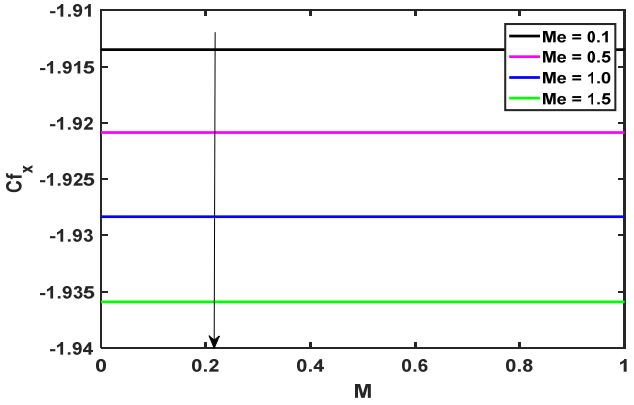

Figure 36. Implementation of Me for Cfx against M

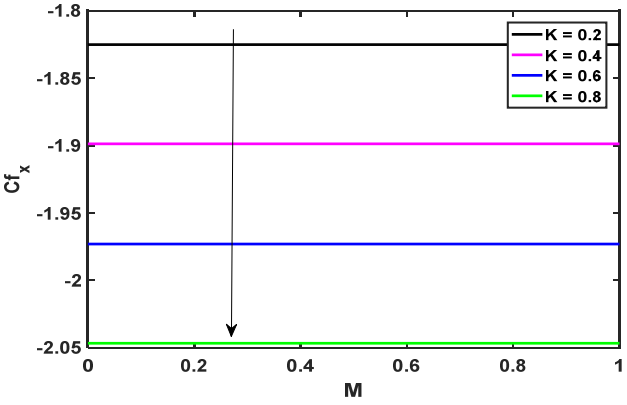

Figure 37. Implementation of K for Cfx against M

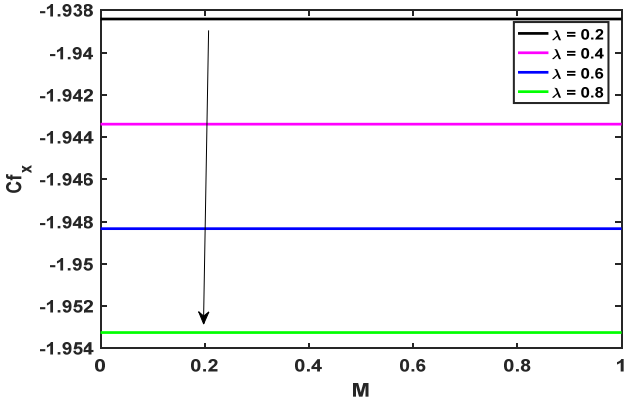

Figure 38. Implementation of λ for Cfx against M

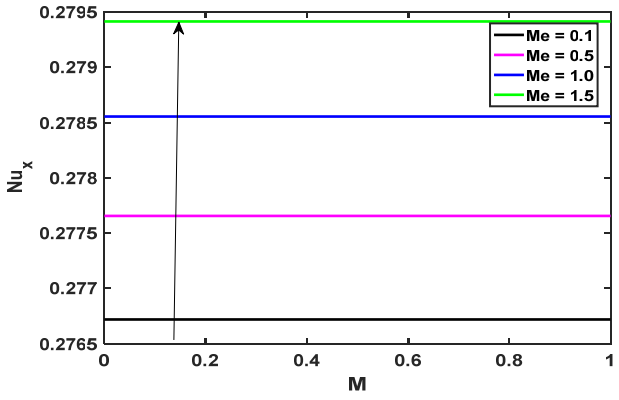

Figure 39. Implementation of Me for Nux against M

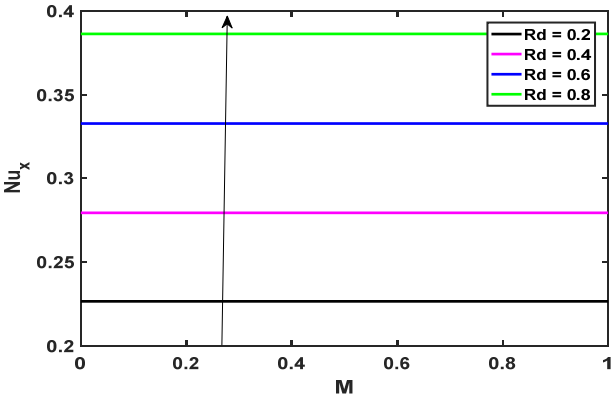

Figure 40. Implementation of Rd for Nux against M

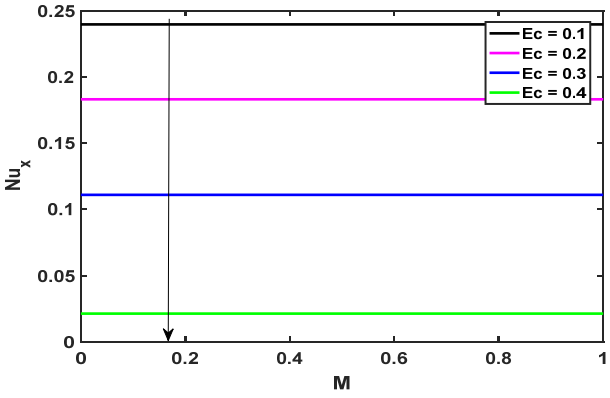

Figure 41. Implementation of Ec for Nux against M

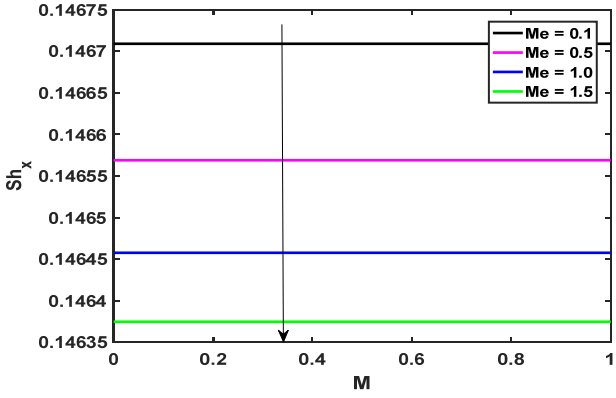

Figure 42. Implementation of Me for Shx against M

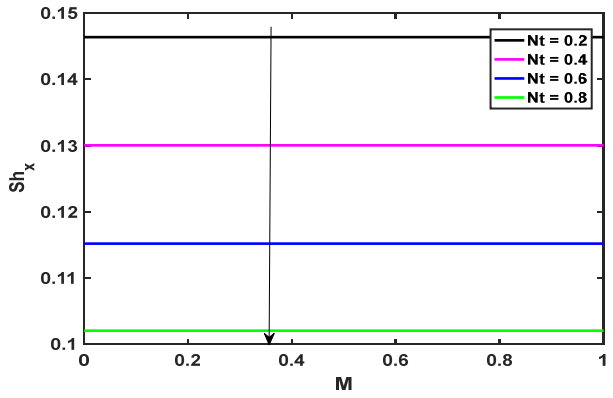

Figure 43. Implementation of Nt for Shx against M

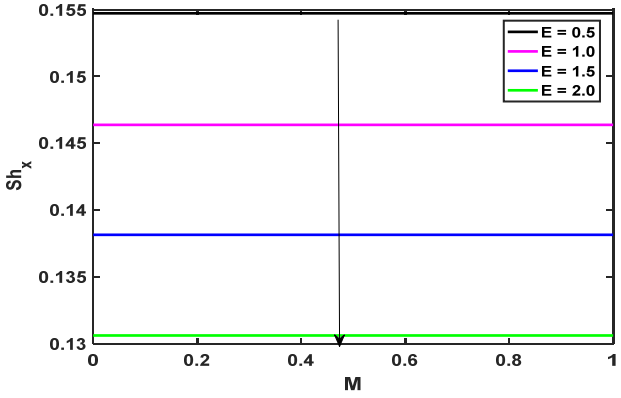

Figure 44. Implementation of E for Shx against M

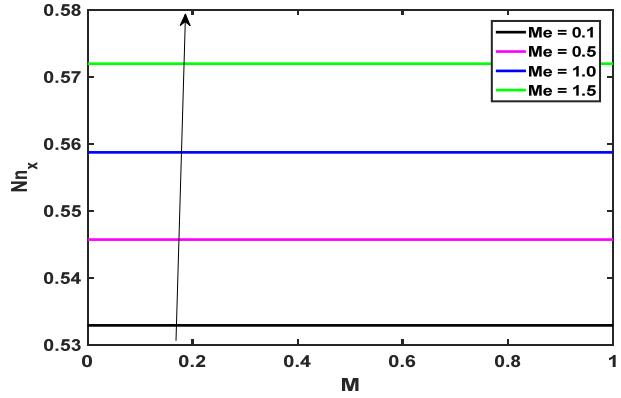

Figure 45. Implementation of Me for Nnx against M

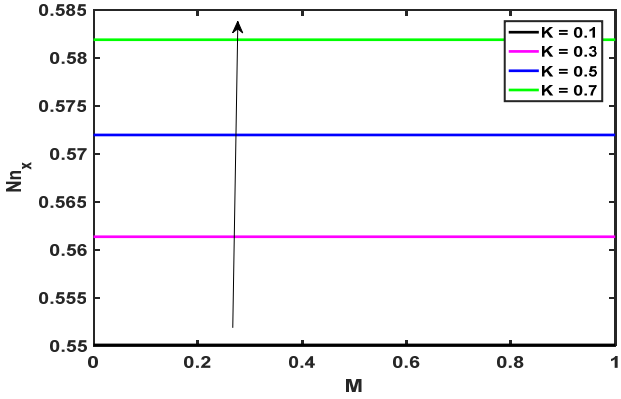

Figure 46. Implementation of K for Nnx against M

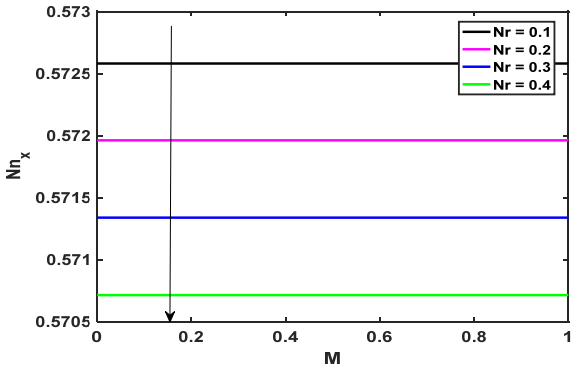

Figure 47. Implementation of Nr for Nnx against M

5. FINAL REMARKS

We have addressed the flow of a viscous, incompressible, micropolar fluid in two-dimensional mixed convective boundary layer through a permeable stretching sheet that is contained in bio-convection, activation energy and melting heat transfer. Assigning numerical values to distinct parameters obtained in the mathematical formulation and displaying the numerical results graphically allows, to gain a physical understanding of the problem by discussing the distributions of velocity $f'(\eta)$, angular velocity $g(\eta)$ (microrotation), temperature $\theta(\eta)$, concentration $\phi(\eta)$ and motile organism $\chi(\eta)$. We have included figures related to local skin friction coefficient τ, couple stress coefficient $h'(0)$, Nusselt number $-\theta'(0)$, Sherwood number $-\phi'(0)$ and micro-organism $-\chi'(0)$. The parameters for bioconvection and the Peclet number both resulted in a decrease in the density of motile gyrotactic microorganisms. The activation energy parameter and the mass biot number both enhance while the Brownian motion parameter and the Lewis number both decrease the concentration profile. Parameters for Brownian motion and thermophoresis, radiation, and the thermal biot number all contribute to a steeper temperature profile.

Data Availability Statement: The datasets used and/or analyzed during the current study are available from the corresponding author upon reasonable request.
Conflict of Interest: Authors have no conflict of Interest at this stage.

ORCID

Sreenivasulu Arigela, https://orcid.org/0009-0003-1591-0138; **A. Shobha,** https://orcid.org/0009-0006-3177-5564; **K. Venkatadri,** https://orcid.org/0000-0001-9248-6180

REFERENCES

[1] S. Mesnage, E.T. Couture, P. Gounon, M. Mock, and A. Fouet, "The capsule and S-layer: two independent and yet compatible macromolecular structures in Bacillus anthracis," J. Bacteriol. **180**, 52–58 (1998). https://doi.org/10.1128/jb.180.1.52-58.1998
[2] D. Kaiser, "Bacterial motility: how do pili pull? Curr. Biol. **10**, 777–780 (2000). https://doi.org/10.1016/S0960-9822(00)00764-8
[3] A.L. Koch, "The sacculus contraction/expansion model for gliding motility." J. Theor. Biol. **142**, 95–112 (1990). https://doi.org/10.1016/S0022-5193(05)80015-3
[4] I.R. Lapidus, and H.C. Berg, "Gliding motility of Cytophaga sp. strain U67," J. Bacteriol. **151**, 384–398 (1982). https://doi.org/10.1128/jb.151.1.384-398.1982
[5] J.W. Costerton, R.G.E. Murray, and C.F. Rabino, "Observations on the motility and the structure of vitreoscilla," Can. J. Microbiol. **7**, 329–339 (1961). https://doi.org/10.1139/m61-040
[6] L.N. Halfen, and R.W. Castenholz, "Gliding in the blue-green alga: a possible mechanism," Nature, **225**, 1163–1165 (1970). https://doi.org/10.1038/2251163a0
[7] B.A. Humphrey, M.R. Dickson, and K.C. Marshall, "Physicochemical and in situ observations on the adhesion of gliding bacteria to surfaces," Arch. Microbiol. **120**, 231–238 (1979). https://doi.org/10.1007/BF00423070
[8] E. Hoiczyk, "Gliding motility in cyanobacteria: observations and possible explanations," Arch. Microbiol. **174**, 11–17 (2000). https://doi.org/10.1007/s002030000187
[9] K. Venkatadri, P. Rajarajeswari, O.A. Bég, V.R. Prasad, H.J. Leonard, and S. Kuharat, "Thermomagnetic Bioconvection Flow in a Semitrapezoidal Enclosure Filled with a Porous Medium Containing Oxytactic Micro-Organisms: Modeling Hybrid Magnetic Biofuel Cells," ASME. J. Heat Mass Transfer. **147**(5): 051201 (2025). https://doi.org/10.1115/1.4067607
[10] R.W. O'Brien, "The gliding motion of a bacterium, Flexibactor strain BH 3," J. Aust. Math. Soc. (Ser B), **23**(1), 2–16 (2009). https://doi.org/10.1017/S0334270000000035
[11] S.T. Islam, and T. Mignot, "The mysterious nature of bacterial surface (gliding) motility: a focal adhesion-based mechanism in Myxococcus xanthus Semin," Cell Dev. Biol. 46, 143–154 (2015). https://doi.org/10.1016/j.semcdb.2015.10.033
[12] B. Nan, and D.R. Zusman, "Novel mechanisms power bacterial gliding motility," Mol. Microbiol. **101**, 186–193 (2016). https://doi.org/10.1111/mmi.13389
[13] A. Shafq, G. Rasool, C.M. Khalique, and S. Aslam, "Second grade bioconvectivenanofuid fow with buoyancy efect and chemical reaction," Symmetry, **12**(4), 621 (2020). https://doi.org/10.3390/sym12040621
[14] E.M.A. Elbashbeshy, H.G. Asker, and B. Nagy, "The effects of heat generation absorption on boundary layer flow of a nanofluid containing gyrotactic microorganisms over an inclined stretching cylinder," Ain. Shams. Eng. J. **13**, 101690 (2022). https://doi.org/10.1016/j.asej.2022.101690
[15] R. Pourrajab, and A. Noghrehabadi, "Bioconvection of nanofluid past stretching sheet in a porous medium in presence of gyrotactic microorganisms with newtonian heating," in: *MATEC Web of Conferences*, **220**, pp. 01004, (EDP Sciences, 2018).
[16] R.R. Kairi, S. Shaw, S. Roy, and S. Raut, "Thermosolutal marangoni impact on bioconvection in suspension of gyrotactic microorganisms over an inclined stretching sheet," J. Heat Transfer, **143**(3), 031201 (2021). https://doi.org/10.1115/1.4048946
[17] K. Li, L. Chen, F. Zhu, and Y. Huang, "Thermal and mechanical analyses of compliant thermoelectric coils for flexible and Bio-Integrated devices," J. Appl. Mech. **88**(2), 021011 (2021). https://doi.org/10.1115/1.4049070
[18] M.V.S. Rao, K. Gangadhar, A.J. Chamkha, and P. Surekha, "Bioconvection in a convectional nanofluid flow containing gyrotactic microorganisms over an isothermal vertical cone embedded in a porous surface with chemical reactive species," Arab J. Sci. Eng. **46**, 2493–2503 (2021). https://doi.org/10.1007/s13369-020-05132-y
[19] A.C. Eringen, "Theory of Thermo-Microfluids," Journal of Mathematical Analysis and Applications, **38**, 480-496 (1972). https://doi.org/10.1016/0022-247X(72)90106-0
[20] G. Ahmadi, "Self-Similar Solution of Incompressible Micropolar Boundary Layer Flow over a Semi-Infinite Plate," International Journal of Engineering Science, **14**, 639-646 (1976). https://doi.org/10.1016/0020-7225(76)90006-9
[21] T. Hayat, M. Mustafa, and S. Obaidat, "Soret and Dufour Effects on the Stagnation Point Flow of a Micropolar Fluid toward a Stretching Sheet," Journal of Fluid Engineering, **133**, 1-9 (2011). https://doi.org/10.1115/1.4003505
[22] M.M. Rahman, "Convective Flows of Micropolar Fluids from Radiate Isothermal Porous Surface with Viscous Dissipation and Joule Heating,' Communications in Nonlinear Science and Numerical Simulation, 14, 3018-3030 (2009). https://doi.org/10.1016/j.cnsns.2008.11.010
[23] G. Lukaszewicz, "Micropolar Fluids: Theory and Applications," (Birkhauser, Boston, 1999). https://doi.org/10.1007/978-1-4612-0641-5
[24] M. Epstein, and D.H. Cho, "Melting heat transfer in steady laminar flow over a fat plate," J. Heat Transfer. **98**, 3 (1976). https://doi.org/10.1115/1.3450595
[25] A. Yacob, A. Ishak, and I. Pop, "Melting heat transfer in boundary layer stagnation-point flow towards a stretching/shrinking sheet in a micropolar fluid," Comput. Fluids, **47**, 16–21 (2011). https://doi.org/10.1016/j.compfluid.2011.01.040
[26] T. Hayat, M. Farooq, A. Alsaedi, and Z. Iqbal, "Melting heat transfer in the stagnation point flow of powell-eyring fluid," J. Thermo Phys. Heat Transfer. **27**(4), 761–766 (2013). https://doi.org/10.2514/1.T4059
[27] W. A. Khan, M. Khan, M. Irfan, and A.S. Alshomrani, "Impact of melting heat transfer and nonlinear radiative heat flux mechanisms for the generalized Burgers fluids," Results Phys. **7**, 4025–4032 (2017). https://doi.org/10.1016/j.rinp.2017.10.004
[28] B. Gireesha, B.M. Shankaralingappa, B.C. Prasannakumara, and B. Nagaraja, "MHD flow and melting heat transfer of dusty Casson fluid over a stretching sheet with Cattaneo Christov heat flux model," Int. J. Ambient Energy, **6**, 1–22 (2020). https://doi.org/10.1080/01430750.2020.1785938

ВПЛИВ СИЛИ ЛОРЕНЦЯ ТА ЕНЕРГІЇ АКТИВАЦІЇ АРРЕНІУСА НА РАДІАЦІЙНИЙ БІОКОНВЕКТИВНИЙ ПЛИН МІКРОПОЛЯРНОЇ НАНОРІДИНИ З ПЛАВЛЕННЯМ НАД ПОВЕРХНЕЮ, ЩО РОЗТЯГУЄТЬСЯ

Сайєд Фазуруддін[a], Срінівасулу Арігела[b], А. Шобха[c], В. Раджа Раджесварі[d], К. Венкатадрі[b]

[a]Факультет технологічної школи математики, Кампус міста знань Аполло Сакета, Мурукамбатту, Університет Аполло Чіттор, Андхра-Прадеш-517127, Індія

[b]Факультет математики, Школа вільних мистецтв і наук, Університет Мохана Бабу (Колишній інженерний коледж Шрі Відьянікетан), Срі Сайнат Нагар, Тірупаті, А.П., 517102, Індія.

[c]Кафедра прикладної математики, Шрі Падмаваті Махіла Вішва Відьялям, Тірупаті 517502, АР, Індія

[d]Кафедра електроніки та комунікаційної техніки, Школа інженерії та технологій, Шрі Падмаваті Махіла Вішва Відьялам, Тірупаті 517502, А.Р., Індія

Новизна цього дослідження полягає у вивченні впливу сили Лоренца, енергії активації Арреніуса та теплопровідності плавлення на поведінку мікрополярної рідини стаціонарного радіаційного біоконвективного потоку мікрополярної нанорідини до розтяжної поверхні. Використовуючи стандартний метод подібності, ми вивели рівняння подібності для відповідних величин імпульсу, кутового моменту, температури та концентрації. Інструмент MATLAB 'bvp4c' використовується для визначення розв'язань перетворених керівних рівнянь. Рівняння подібності у чотирьох вимірах (імпульс, кутовий момент, температура та концентрація) розв'язані чисельно. Ми дослідили поведінку полів мікрообертання, швидкості, концентрації та температури для різних параметрів. Результати показують, що щільність рухомості мікроорганізмів зменшується зі збільшенням числа Пекле та параметра різниці концентрацій мікроорганізмів. Щільність рухомості збільшується зі збільшенням числа Пекле в мікробних концентраціях. Тому нанорідини є придатними як рідини для теплопередачі завдяки їхньому ефекту охолодження поверхні. Застосована числова схема підтверджена шляхом порівняння з попередніми числовими значеннями.

Ключові слова: *теплопередача плавлення; мікрополярна нанорідина; біоконвекція; радіаційний тепловий потік; енергія активації*